Indirect Grid Current Control of *LCL* Filter based Grid-Connected Converter

Subhajyoti Mukherjee
Infineon Technologies
Warwick, RI
email: Subhajyoti.Mukherjee@infineon.com

Pourya Shamsi, Mehdi Ferdowsi and Jonathan Kimball
Department of Electrical and Computer Engineering
Missouri University of Science and Technology
Rolla, MO, USA
emails: shamsip@mst.edu, ferdowsi@mst.edu, kimballjw@mst.edu

***Abstract*-- This paper presents a method to indirectly control the grid current of a grid connected converter interfaced with a *LCL* filter. The proposed method is based on estimating the fundamental and harmonic components of the current drawn by the filter capacitor. The estimated fundamental and harmonic components of the filter capacitor current are then compensated by injecting an equal amount of current from the converter side using a well-designed current controller. This indirectly ensures the grid current to be at the desired power factor and immune to any distortions in the grid voltage. The proposed estimation and control scheme is verified by experimental results.**

***Index Terms*— Grid connected converter, *LCL* filter, sensor less control, voltage estimation, harmonic compensation.**

I. Introduction

Power electronic converters are generally interfaced to the grid using either an *L* filter or an *LCL* filter. Optimally designed *LCL* filters substantially reduce the switching harmonics in the grid side current compared to the *L* filter [1]. However, the control of the converter with an *LCL* filter is more challenging compared to a converter interfaced with only the *L* filter [2]. A single-phase grid connected converter with an *LCL* filter is shown in Fig. 1. In the figure, L_i is the converter side filter inductance (with winding resistance r_i), C is the filter capacitance, L_g is the grid side filter inductance (with winding resistance r_g), i_L is the converter current, i_g is the grid current, i_c is the capacitor current, v_c is the voltage across the filter capacitor, v_g is the grid voltage, and v_i is the output of the bridge. In such a configuration, the transfer function of the converter side current i_L to the output voltage of the bridge v_i, presents an equivalent first order system [3], [4] while the transfer function of the grid current, i_g, to v_i, presents a third order system [3], [4] (see Fig. 2). Typical system parameters are given in the Appendix.

Direct control of the grid current implies designing a controller for a third order system, which generally involves multiple control loops [2], [5]−[9]. In general, the grid side current is chosen as the variable for the outer loop while the inner loop variable is chosen as the capacitor current [2], [5], [6] or the converter current [7] or the filter capacitor voltage

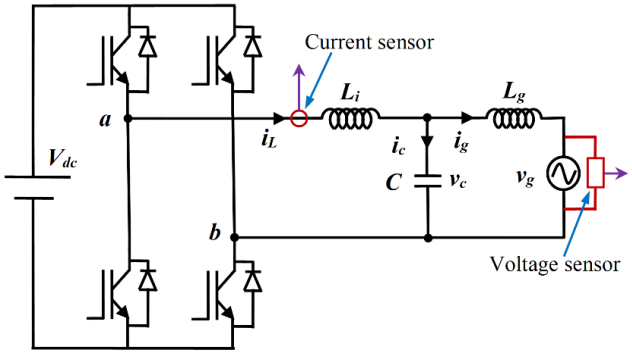

Fig. 1. A single-phase grid connected inverter with *LCL* filter.

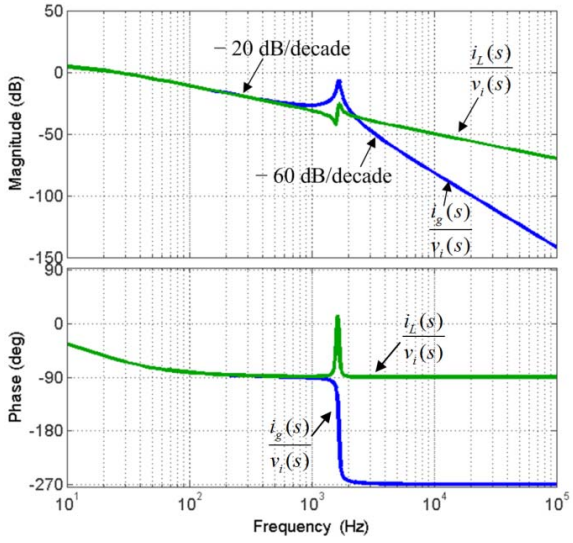

Fig. 2. The frequency response of $\frac{i_L(s)}{v_i(s)}$ and $\frac{i_g(s)}{v_i(s)}$.

[8], [9]. Multi loop control structure for *LCL* filter based grid connected converter has been proposed in [2], [5], [10]− [14]. However, these are based on pole zero cancellation or parameter dependent. A direct grid current control using resonant controllers to mitigate grid voltage disturbance has

been suggested in [15]. However, the proposed controller needs zero compensation for stability.

Compared to direct control of the grid current, controlling the converter current is simple as it presents an equivalent first order system [3], [4]. However, it is generally not preferred as the filter capacitor draws a reactive current which being unknown cannot be compensated by controlling the converter current [1]. This leads to a deviation in the desired power supplied to the grid, especially at low load conditions. Further, due to the presence of the capacitor branch, the grid current is affected by the harmonics and distortions in the grid voltage. Addressing this problem, this paper proposes to estimate the filter capacitor current and then control the grid side current by controlling the converter side current and supplying the required capacitive reactive power (both fundamental and harmonics) from the converter side. The proposed scheme uses only one current sensor (to measure i_L) and one voltage sensor to measure the grid voltage, v_g.

The rest of the paper is arranged as follows. The estimation of the filter capacitor current and the proposed control structure is presented in Section II. The detailed stability analysis and controller design guidelines of the proposed estimation is presented in Section III. The results are discussed in Section IV and the conclusion presented in Section V.

II. Control Architecture

The overall control block diagram of the proposed control of the *LCL* filter based inverter is shown in Fig. 3. The control structure incorporates the estimation of the fundamental and harmonic components of the filter capacitor voltage, reference generation that includes the computation of the filter capacitor current, and a current controller for the converter side inductor current. Only i_L and v_g are measured. The idea is to estimate the filter capacitor current (fundamental and harmonic components) and then add it to the desired grid current reference to generate the converter current reference i_{Lref}. A current controller then ensures that the converter side current i_L tracks i_{Lref}. In Fig. 3, v_i is the output of the current controller, P_{ref} and Q_{ref} are the reference values of the active and reactive power, cosθ and sinθ are the unit vectors generated from the phase locked loop (PLL) while ω_g is the grid frequency as obtained from the PLL structure.

A. Estimation of the filter capacitor voltage

The estimation of the fundamental and harmonic components of the filter capacitor current, which is critical to the operation of the inverter, uses the estimated fundamental and harmonic components of the filter capacitor voltage. The proposed voltage estimation is based on the active and reactive power transferred from the converter bridge to the filter capacitor, similar to as in [16], [17]. For the instantaneous computation of the average power in a single-phase system, the active and reactive powers are calculated in a fictitious two phase ($\alpha\beta$) frame of reference. The in-phase (α axis) and quadrature (β axis) signals are generated using the well-known second order generalized integrators (SOGI) [18], [19]. The SOGI structure compromises two filters, a low

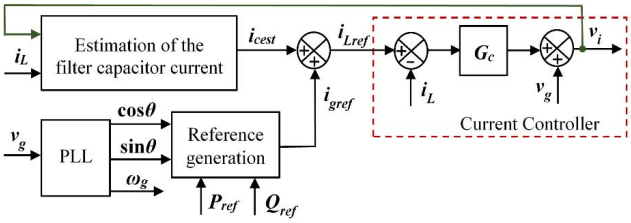

Fig. 3. Overall block diagram of the proposed control scheme.

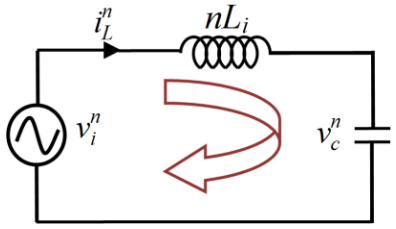

Fig. 4. Equivalent circuit representation from the converter bridge to the filter capacitor of the circuit in Fig. 1.

pass filter and a band pass filter. Details of the SOGI structure are well established in the existing literature and are not repeated here. The generalized equivalent circuit relating v_i and v_c for the n^{th} harmonic is shown in Fig. 4. The voltage drop across the switches, on-state resistance and resistive impedance of the cables being small have been neglected in the equivalent circuit of Fig. 4. The superscript n denotes the n^{th} harmonic component in Fig. 4.

For the circuit shown in Fig. 4, the active and reactive power (P and Q respectively) delivered by the source v_i^n to the source v_c^n are given as

$$P_{i1}^n = \frac{1}{2}\left(v_{i\alpha}^n i_{L\alpha}^n + v_{i\beta}^n i_{L\beta}^n\right) \quad (1)$$

$$Q_{i1}^n = \frac{1}{2}\left(v_{i\beta}^n i_{L\alpha}^n - v_{i\alpha}^n i_{L\beta}^n\right) \quad (2)$$

Also, for two sources (in this case v_i^n to v_c^n) connected through a pure inductance (in this case nL_i), the active and reactive power supplied from the source v_i^n to v_c^n are given as

$$P_{i2}^n = \frac{V_i^n V_c^n \sin\delta_i^n}{2nX_i} \quad (3)$$

$$Q_{i2}^n = \frac{V_i^n}{2nX_i}(V_i^n - V_c^n \cos\delta_i^n) \quad (4)$$

where, $v_i^n = V_i^n \angle\varepsilon_i^n$, $v_c^n = V_c^n \angle\left(\varepsilon_i^n - \delta_i^n\right)$ and $X_i = \omega_g L_i$

In (3)-(4) V_{i1}^n and V_c^n are the peak values of the voltage vectors v_{i1}^n and v_c^n respectively while δ_i^n is the angle v_i^n and v_c^n. The active power computed by both (1) and (3) must be identical. Observing (1), all the variables on the right side of the equation are known (measured or computed). Similarly, all variables in (3) are also known except the term $V_c^n \sin\delta_i^n$. Based on this, a closed loop estimation of $V_c^n \sin\delta_i^n$ is proposed as shown in Fig. 5. Similarly, the reactive power given by (2) and (4) are identical. Hence (2) and (4) are used to estimate $V_c^n \cos\delta_i^n$. The closed loop estimation of $V_c^n \cos\delta_i^n$ is shown in Fig. 6. The estimated values $(V_c^n \sin\delta_i^n)_{est}$ and $(V_c^n \cos\delta_i^n)_{est}$ are used to give an estimate of the voltage v_c^n as discussed below.

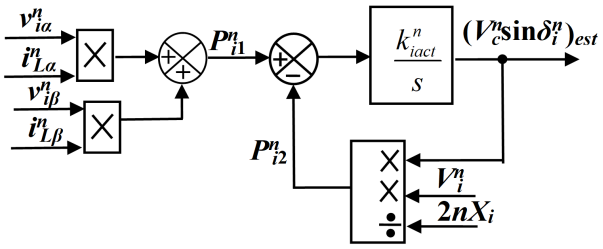

Fig. 5. Proposed closed loop estimation structure to estimate $V_c^n \sin\delta_i^n$.

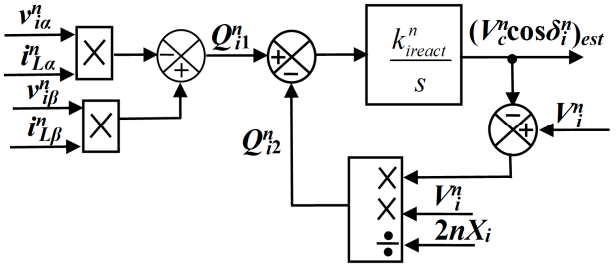

Fig. 6. Proposed closed loop estimation structure to estimate $V_c^n \cos\delta_i^n$.

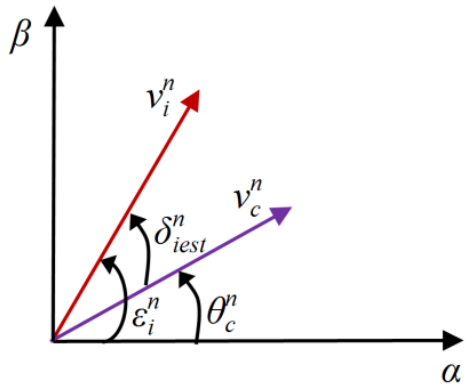

Fig. 7. Representation of the different voltage vector in the α-β frame of reference.

The phasors v_i^n *and* v_c^n are represented in Fig. 7. The unit vectors $\cos\varepsilon_i^n$ and $\sin\varepsilon_i^n$ can be found as

$$\cos\varepsilon_i^n = \frac{v_{i\alpha}^n}{V_i^n} \text{ and } \sin\varepsilon_i^n = \frac{v_{i\beta}^n}{V_i^n} \tag{5}$$

where $$V_i^n = \sqrt{\left(v_{i\alpha}^n\right)^2 + \left(v_{i\beta}^n\right)^2} \tag{6}$$

Again, unit vectors $\cos\delta_{iest}^n$ and $\sin\delta_{iest}^n$ are found as

$$\cos\delta_{iest}^n = \frac{\left(V_c^n \cos\delta_i^n\right)_{est}}{V_{cest}^n} \tag{7}$$

and $$\sin\delta_{iest}^n = \frac{\left(V_c^n \sin\delta_i^n\right)_{est}}{V_{cest}^n} \tag{8}$$

where, $V_{cest}^n = \sqrt{\left((V_c^n \cos\delta_i^n)_{est}\right)^2 + \left((V_c^n \sin\delta_i^n)_{est}\right)^2}$

Angle θ_c^n can be expressed as $\varepsilon_i^n - \delta_{iest}^n$ (see Fig. 7). Unit vectors $\cos\theta_c^n$ and $\sin\theta_c^n$ are then computed as

$$\cos\theta_c^n = \cos\varepsilon_i^n \cos\delta_{iest}^n + \sin\varepsilon_i^n \sin\delta_{iest}^n \tag{9}$$

$$\sin\theta_c^n = \sin\varepsilon_i^n \cos\delta_{iest}^n - \cos\varepsilon_i^n \sin\delta_{iest}^n \tag{10}$$

Unit vectors $\cos\theta_c^n$ and $\sin\theta_c^n$ as in (9) and (10) are used to compute the α-axis and β-axis fundamental component of the filter capacitor voltage as given below

$$v_{cest\alpha}^n = V_{cest}^n \cos\theta_c^n \tag{11}$$

$$v_{cest\beta}^n = V_{cest}^n \sin\theta_c^n \tag{12}$$

One limitation of the proposed estimation approach is that the converter side inductor is lossless, linear, and known precisely. This approximation is reasonable for well-designed systems, in which reactance dominates over resistance (particularly at higher harmonic frequencies) and the nominal conditions are far from saturation. Alternatively, virtual flux based voltage estimation methods have been presented in literature [20]-[22]. The virtual flux based estimation method involves an integration operation. A pure integrator has dc drift problems. Hence the integration is generally performed by a low pass filter. However, low pass filtering is always associated with phase lag and attenuation in the gain.

B. Stability Analysis of the Proposed Estimation

The stability of the estimation as in Fig. 5 is analyzed using Lyapunov analysis. A candidate Lyapunov function is proposed as

$$V_P = \frac{1}{2}\left(V_c^n \sin\delta_i^n\right)_{err}^2 \tag{13}$$

where $$\left(V_c^n \sin\delta_i^n\right)_{err} = \left(V_c^n \sin\delta_i^n\right) - \left(V_c^n \sin\delta_i^n\right)_{est} \tag{14}$$

Clearly, if we take $x = \left(V_c^n \sin\delta_i^n\right)_{err}$ as the state variable, $V_P(x)$ is positive definite and radially unbounded. Taking the derivative of both sides in (13) yields

$$\dot{V}_P = \left(V_c^n \sin\delta_i^n\right)_{err} \frac{d}{dt}\left(V_c^n \sin\delta_i^n\right)_{err} \tag{15}$$

Using (14) in (15),

$$\dot{V}_P = -\left(V_c^n \sin\delta_i^n\right)_{err} \frac{d}{dt}\left(V_c^n \sin\delta_i^n\right)_{est} \tag{16}$$

Defining $P_{err} = P_1 - P_2$, Fig. 5 gives

$$\frac{d}{dt}\left(V_c^n \sin\delta_i^n\right)_{est} = k_{iact}^n P_{err}^n \tag{17}$$

Using expressions for P_1 and P_2, P_{err} can also be expressed as

$$P_{err}^n = P_1^n - P_2^n = \frac{V_i^n}{2nX_i}\left(\left(V_c^n \sin\delta_i^n\right) - \left(V_c^n \sin\delta_i^n\right)_{est}\right) \tag{18}$$

or, $$P_{err}^n = \frac{V_i^n}{2nX_i}\left(V_c^n \sin\delta_i^n\right)_{err} \tag{19}$$

Using (17) and (19) in (16) results in

$$\dot{V}_P = -k_{iact}^n \frac{V_i^n}{2nX_i}\left(V_c^n \sin\delta_i^n\right)_{err}^2 \tag{20}$$

Equation (20) proves that the derivative of the Lyapunov function as in (13) is always negative. The proposed Lyapunov function satisfies all the required conditions for global stability, so the estimation proposed in Fig. 5 is stable. Similar analysis can be done to prove that the estimation method in Fig. 6 is globally stable.

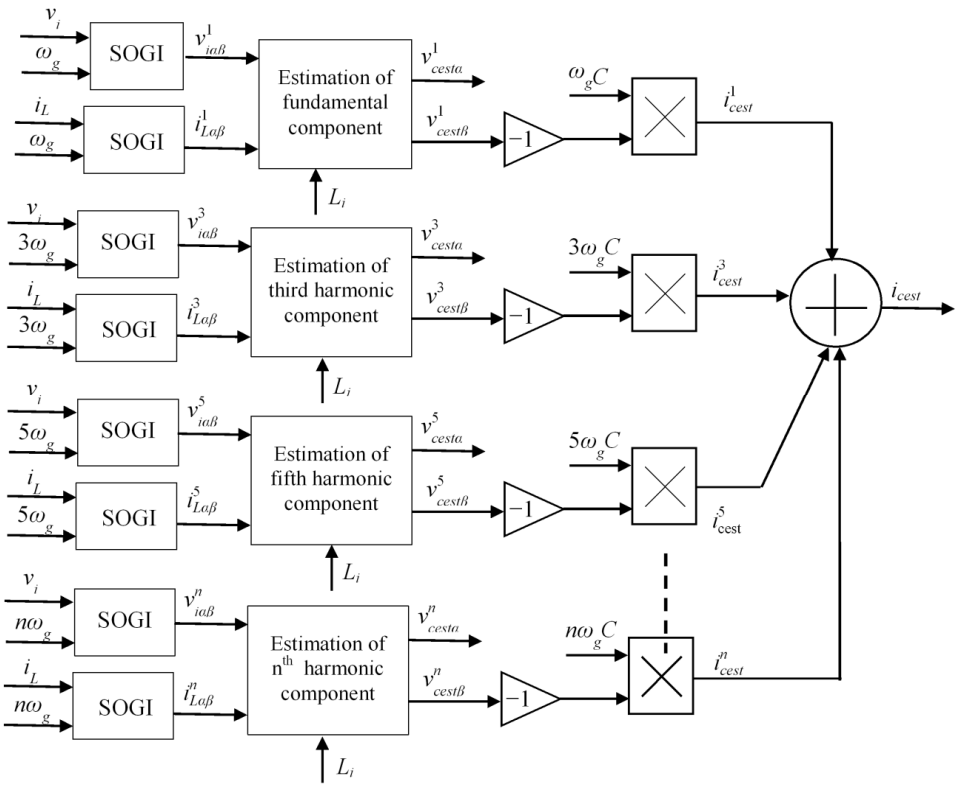

Fig. 8. Estimation of the filter capacitor current.

C. Estimation of the filter capacitor current

The estimation of the filter capacitor current is shown in Fig. 8. Once the β-axis component of the capacitor voltage is estimated, the proposed controller uses the estimated capacitor value to compensate the reactive current drawn by the capacitor (see Fig. 3). The fundamental component of the filter capacitor current can be found as

$$i_{cest} = C\frac{dv^1_{cest}}{dt} \tag{21}$$

$$i_{cest} = -\omega_g C v^1_{cest\beta} \tag{22}$$

Generally, metallized polypropylene film capacitors are chosen as the filter capacitor of the *LCL* filter. These capacitors show negligible deviations in the capacitance value over temperature and time. In addition, these capacitors have negligible equivalent series resistance (ESR), hence any resistive drop has been ignored in (21). Compensating the capacitor current as in (22) is sufficient to ensure the desired power factor of the grid current. However, generally the grid voltage is contaminated with harmonics. To reduce the distortions in the grid current, in addition to the fundamental component of the capacitor current, harmonics of the capacitor current need to be compensated. The harmonic component of the β-axis component of the filter capacitor voltage being known, the corresponding harmonic filter capacitor current can be easily computed. Including the effect of the harmonics, the capacitor current as in (22) is modified and given as

$$i_{cest} = -\sum_{n=1,3,5,7\ldots}\left(n\omega_g C\right)v^n_{cest\beta} \tag{23}$$

Only odd harmonic components have been considered in (23) because even harmonics are typically absent in grid voltages. Furthermore, higher order harmonics (beyond the 13th harmonic) are negligible in practical grid voltages.

As depicted in Fig. 3, i_{cest} as in (23) is added to the grid current reference (i_{gref}) to generate the converter current reference i_{Lref}.

$$i_{Lref} = i_{gref} + i_{cest} \tag{24}$$

A proportional resonant controller, with resonant peaks at the fundamental and dominant harmonic frequencies is then employed to track current reference i_{Lref}. The control law is defined as

$$v_i(s) = \left(i_{Lref}(s) - i_L(s)\right)G_c(s) + v_g(s) \tag{25}$$

$$\text{where, } G_c = k_p + \sum_{n=1,3,5,7\ldots}\frac{k_{rn}\omega_{cutn}s}{s^2 + 2\omega_{cutn}s + (n\omega)^2} \tag{26}$$

The control structure given as in (26) is a proportional multi-resonant controller. With the control law as in (25), response of i_L to i_{Lref} is given as (derivation shown in Appendix, Eq. (A9))

$$i_L(s) = \frac{\left(1+H_2H_3\right)G_c(s)}{\left(\left(1+H_2H_3\right)\left(H_1+G_c(s)\right)+H_2\right)}i_{Lref}(s) + \frac{H_2H_3}{\left(\left(1+H_2H_3\right)\left(H_1+G_c(s)\right)+H_2\right)}v_g(s) \tag{27}$$

TABLE I
CONTROLLER PARAMETERS

k_p (V/A)	40
k_{r1} (V/Asec)	1,000
k_{r3} (V/Asec)	1,500
k_{r5} (V/Asec)	2,000
k_{r7} (V/Asec)	3,000
ω_{cut1} (rad/sec)	10
ω_{cut3} (rad/sec)	15
ω_{cut5} (rad/sec)	20
ω_{cut7} (rad/sec)	30

From (27) the loop gain of the current controller is given as

$$G_{ol}(s) = \frac{(1+H_2H_3)G_c(s)}{H_1 + H_2 + H_1H_2H_3} \tag{28}$$

The response of the grid current is then given as (derivation shown in Appendix, Eq. (A20))

$$i_g(s) = \frac{(1+H_2H_3)G_c(s)}{D(s)} i_{gref}(s) + \frac{H_2H_3}{D(s)} v_g(s) + \left(\frac{(1+H_2H_3)G_c(s)}{D(s)} - 1 \right) i_{cest}(s) - i_{cest}^{'}(s) \tag{29}$$

Equations (27)-(29) are derived in detail in the Appendix. In (29), $i_{cest}^{'}$ is the uncompensated part of the filter capacitor current. The frequency response of the current controller and the plant (the loop gain as in (28)) for the controller parameters as listed in Table I are shown in Fig. 9. The effective first order nature of the system helped to achieve a high open loop crossover frequency of 2.8 kHz with a phase margin of 81°. The response of the controller to the estimated components of the capacitor current is shown in Fig. 10. It is seen that the gain at the fundamental and compensated harmonic frequencies is very less. The uncompensated capacitor current cannot be attenuated. Its effect is reflected in the grid current. However, the uncompensated portion of the filter capacitor current is composed of higher order harmonic current. These harmonics will be contributed by higher order harmonics in the grid voltage which are of negligible magnitude in practical grid voltage. The grid voltage also acts as a disturbance input on the grid current (refer (29)). The frequency response of the output admittance relating the effect of the grid voltage to the grid current (as obtained from (29)) is shown in Fig. 11. The figure shows that the admittance is sufficiently attenuated at the harmonic and high frequencies.

III. RESULTS

The proposed control scheme was experimentally verified on a scaled down prototype of 400 VA converter. The grid voltage was maintained at 100 V rms. Experimental results are reported for a reference of 0.5 p.u. active power (corresponding to 2 A grid current) and 0 p.u. of reactive power, respectively. The proposed capacitor current compensation was enabled after a delay. The grid voltage, converter current and grid current waveforms are shown in

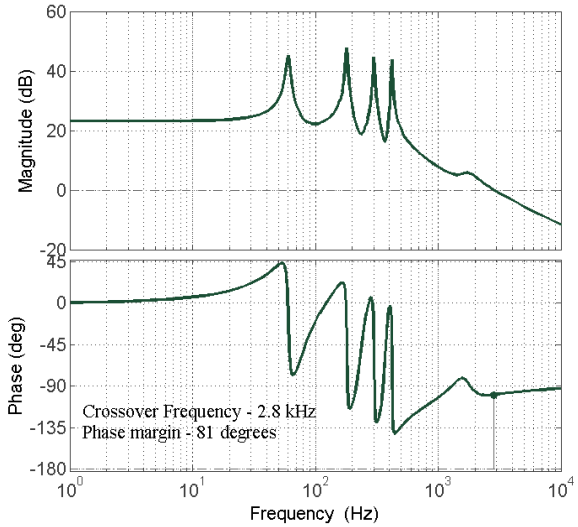

Fig. 9. Loop gain plot of the current controller and plant.

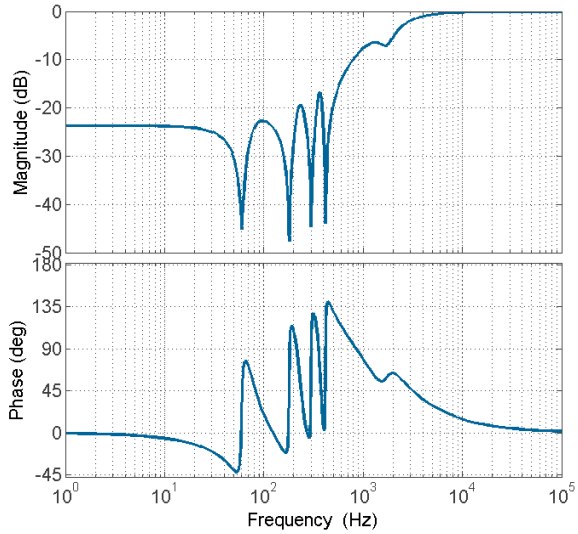

Fig. 10. Frequency response showing the effect of the filter capacitor current on the grid current.

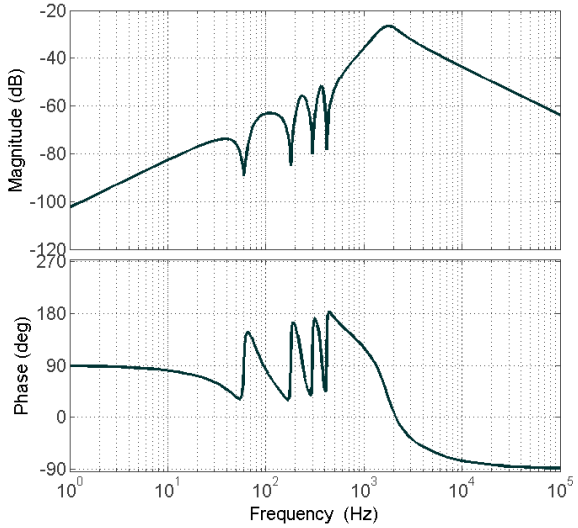

Fig. 11. Frequency response of the output admittance.

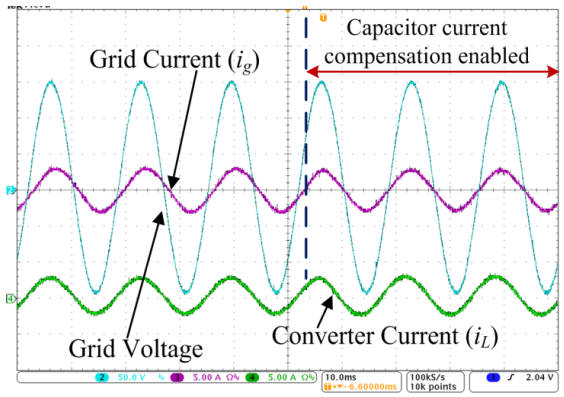

Fig. 12. Grid voltage, grid current and converter current with and without the proposed capacitor current compensation under normal grid conditions.

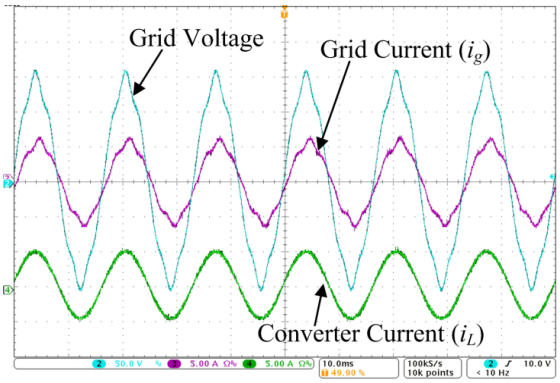

Fig. 13. Grid voltage, grid current and converter current without compensation of the capacitor current under distorted grid conditions.

Fig. 12. While the capacitor current compensation was disabled, unity power factor operation was not ensured. The grid is supplying about 75 VAR of reactive power. However, as soon as the proposed capacitor current compensation is enabled the grid current becomes in phase with the grid voltage ensuring unity power factor operation. No instability with the proposed control is noted during the transition.

The grid voltage is now mixed with 5% of fifth harmonic and 3% seventh harmonic voltage. The waveforms without compensation of the filter capacitor current are shown in Fig. 13. It is observed from the figure that the grid current is not in phase with the grid voltage. Additionally, as the harmonic components of the capacitor current are not compensated, the grid current is distorted. Measurements report a THD of 6.8%.

The fundamental and harmonic compensation of the capacitor current are implemented next. The corresponding waveforms are shown in Fig. 14. It can be seen from Fig. 14 that with the proposed harmonic compensation the grid current has less distortion (THD of 2.3%). The actual filter capacitor voltage and the estimated fundamental, fifth and seventh harmonic components as obtained from the estimation algorithm are shown in Fig. 15. The waveforms with the proposed control architecture during a transition in active power from 0.25 p.u to 1 p.u are shown in Fig. 16. The entire system was stable and the proposed controller ensures good tracking of the grid current during the transition. The

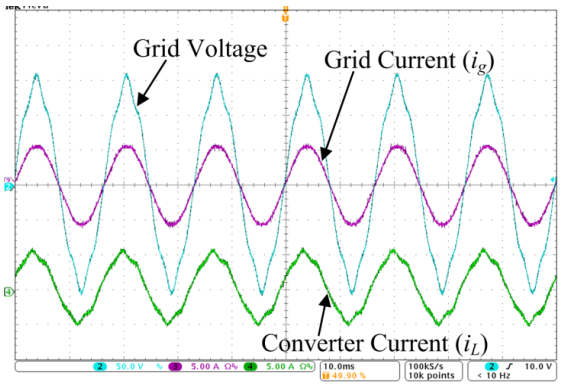

Fig. 14. Grid voltage, grid current and converter current with proposed compensation of the fundamental and harmonic capacitor current under distorted grid conditions.

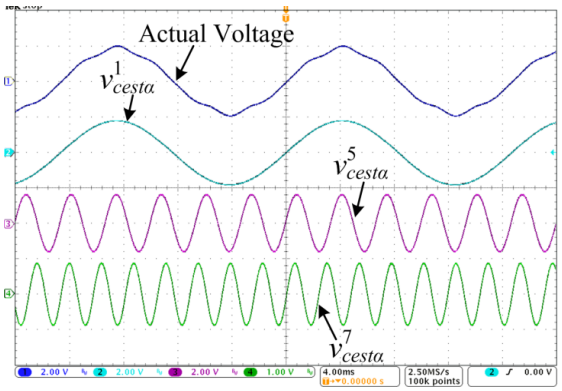

Fig. 15. The actual capacitor voltage, estimated fundamental (v^1_{cesta}), fifth harmonic (v^5_{cesta}) and seventh harmonic (v^7_{cesta}) components. (Scale : Actual voltage : 150V/div, Estimated fundamental : 150 V/div, Fifth harmonic : 10V/div, Seventh harmonic : 5.25V/div).

waveforms during a sag in the grid voltage by 20% are reported in Fig. 17. The waveforms show that the proposed control could ensure satisfactory performance during sudden change in the grid voltage with negligible distortions in the grid current.

IV. Conclusion

This paper presented a control architecture to control the grid side current of a grid connected converter with *LCL* filter by estimating the filter capacitor current. The filter capacitor voltage was first estimated, and the filter capacitor current was computed from the estimated filter capacitor voltage. The estimated fundamental and harmonic components of the filter capacitor current were then compensated from the converter side, thereby maintaining a sinusoidal grid current at the desired power factor. Experimental results showed the efficacy of the proposed estimation and control scheme in controlling the current supplied to the grid.

Appendix

The detailed derivation of the transfer function presented in (27)-(29) are given below. The transfer functions are derived referenced to the circuit in Fig. 1 and the control architecture in Fig. 3. In the Laplace domain, inductor current, capacitor voltage and grid current dynamics are given as

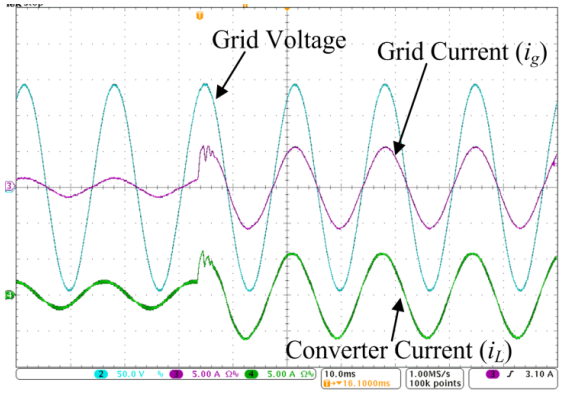

Fig. 16. Grid voltage, grid current and converter current during a transition from 0.25 p.u to 1 p.u of active power.

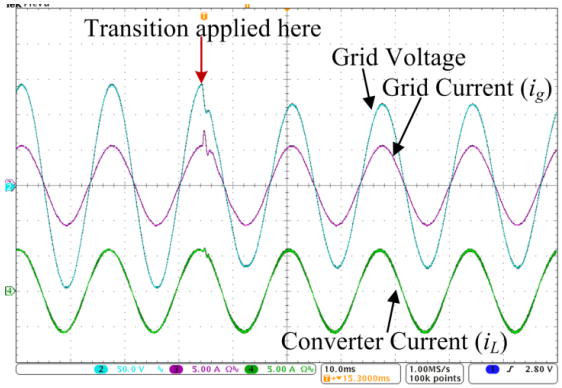

Fig. 17. Grid voltage, grid current and converter current during a transition of 20% in the grid voltage.

$$(sL_i + r_i) i_L(s) = v_i(s) - v_c(s) \quad \text{(A1)}$$

$$(sL_g + r_g) i_g(s) = v_c(s) - v_g(s) \quad \text{(A2)}$$

$$sC(v_c(s) - i_c(s)R_c) = i_c(s) \quad \text{(A3)}$$

$$i_c(s) = i_L(s) - i_g(s) \quad \text{(A4)}$$

In (A1), R_c is the series resistance with the filter capacitor. Let, $H_1 = (sL_i+r_i)$, $H_2 = (sL_g+r_g)$ and $H_3 = sC/(1+sCR_c)$. Using (A1) in the controller structure as in (17) yields

$$\left(i_{Lref}(s) - i_L(s)\right) G_c(s) + v_g(s) = H_1 i_L(s) + v_c(s) \quad \text{(A5)}$$

Using (A3) and (A4) in (A2) to eliminate i_g one gets

$$\left(i_{Lref}(s) - i_L(s)\right) G_c(s) + v_g(s) = H_1 i_L(s) + v_c(s) \quad \text{(A6)}$$

$$v_c(s) = \frac{H_2 i_L(s) + v_g(s)}{1 + H_2 H_3} \quad \text{(A7)}$$

Using (A6) in (A5) yields

$$\left(i_{Lref}(s) - i_L(s)\right) G_c(s) + v_g(s) = H_1 i_L(s) + \frac{H_2 i_L(s) + v_g(s)}{1 + H_2 H_3} \quad \text{(A8)}$$

or,

$$i_L(s) = \frac{(1 + H_2 H_3) G_c(s)}{\left((1 + H_2 H_3)(H_1 + G_c(s)) + H_2\right)} i_{Lref}(s) + \frac{H_2 H_3}{\left((1 + H_2 H_3)(H_1 + G_c(s)) + H_2\right)} v_g(s) \quad \text{(A9)}$$

From (A8), the closed loop transfer function relating i_L and i_{Lref} is given as

$$G_{cl}(s) = \frac{(1 + H_2 H_3) G_c(s)}{\left((1 + H_2 H_3)(H_1 + G_c(s)) + H_2\right)} \quad \text{(A10)}$$

Arranging (A9) in the standard form one gets

$$G_{cl}(s) = \frac{\frac{(1 + H_2 H_3) G_c(s)}{H_1 + H_2 + H_1 H_2 H_3}}{1 + \left(\frac{(1 + H_2 H_3) G_c(s)}{H_1 + H_2 + H_1 H_2 H_3}\right)} \quad \text{(A11)}$$

From (A10) the open loop transfer function is given as

$$G_{ol}(s) = \frac{(1 + H_2 H_3) G_c(s)}{H_1 + H_2 + H_1 H_2 H_3} \quad \text{(A12)}$$

Observing (A11) the plant transfer function is obtained as

$$G_p(s) = \frac{1 + H_2 H_3}{H_1 + H_2 + H_1 H_2 H_3} \quad \text{(A13)}$$

The response of the grid current is found next. i_L and i_{Lref} can be represented as

$$i_L(s) = i_g(s) + i_c(s) \quad \text{(A14)}$$

$$i_{Lref}(s) = i_{gref}(s) + i_{cest}(s) \quad \text{(A15)}$$

Using (A13) and (A14) in (A8) yields

$$i_g(s) + i_c(s) = \frac{(1 + H_2 H_3) G_c(s)}{D(s)} \left(i_{gref}(s) + i_{cest}(s)\right) + \frac{H_2 H_3}{D(s)} v_g(s) \quad \text{(A16)}$$

where, $D(s) = (1 + H_2 H_3)(H_1 + G_c(s)) + H_2$ (A17)

Considering i_c to be combined of n harmonics, out of which k harmonics are compensated by i_{cest}

$$i_c = i_{cest} + i'_{cest}(s) \quad \text{(A18)}$$

$$i_{cest} = \sum_{j=1}^{k} i_{cj} \text{ and } i'_{cest}(s) = \sum_{j=k+1}^{n} i_{cj} \quad \text{(A19)}$$

Using (A17) and (A18) in (A15) yields

$$i_g(s) = \frac{(1 + H_2 H_3) G_c(s)}{D(s)} i_{gref}(s) + \frac{H_2 H_3}{D(s)} v_g(s) + \left(\frac{(1 + H_2 H_3) G_c(s)}{D(s)} - 1\right) i_{cest}(s) - i'_{cest}(s) \quad \text{(A20)}$$

System Parameters: L_i = 2.5 mH, L_g = 0.5 mH, r_i = 0.04Ω, r_g = 0.01Ω, C = 20μF.

REFERENCES

[1] M. Liserre, F. Blaabjerg, and S. Hansen, "Design and control of an LCL- filter-based three-phase active rectifiers," *IEEE Trans. Ind. Appl.*, vol. 41, no. 5, pp. 1281–1291, Sep./Oct. 2005.

[2] E. Twining and D. G. Holmes, "Grid current regulation of a three-phase voltage source inverter with an LCL input filter," *IEEE Trans. Power Electron.*, vol. 18, no. 3, pp. 888–895, May 2003.

[3] B. Bolsens, K. De Brabandere, J. Van den Keybus, R. Belmans, and J. Driesen, "Model-based generation of low distortion currents in grid coupled PWM-Inverters using an LCL output filter," *IEEE Trans. Power Electron.*, vol. 21, no. 4, pp. 1032–1040, Jul. 2006.

[4] G. Shen, D. Xu, L. Cao, and X. Zhu, "An improved control strategy for grid-connected voltage source inverters with an LCL filter," *IEEE Trans. Power Electron.*, vol. 23, no. 4, pp. 1899–1906, Jul. 2008.

[5] L. Fei, Z. Yan, D. Shanxu, Y. Jinjun, L. Bangyin, and L. Fangrui, "Parameter design of a two-current-loop controller used in a grid-connected inverter system with LCL filter," *IEEE Trans. Ind. Electron.*, vol. 56, no. 11, pp. 4483–4491, Nov. 2009.

[6] C. Bao, X. Ruan, X. Wang, W. Li, D. Pan, and K. Weng, "Step by-step controller design for LCL-type grid-connected inverter with capacitor–current-feedback active-damping," *IEEE Trans. Power Electron.*, vol. 29, no. 3, pp. 1239–1253, Mar. 2014.

[7] X. Zhang, J. W. Spencer, and J. M. Guerrero, "Small-signal modeling of digitally controlled grid-connected inverters with LCL filters," *IEEE Trans. Ind. Electron.*, vol. 60, no. 9, pp. 3752–3765, Sep. 2013.

[8] J. Dannehl, F. W. Fuchs, S. Hansen, and P. B. Thøgersen, "Investigation of active damping approaches for PI-based current control of grid-connected pulse width modulation converters with LCL filters," *IEEE Trans. Ind. Appl.*, vol. 46, no. 4, pp. 1509–1517, Jul./Aug. 2010.

[9] R. Peña Alzola, M. Liserre, F. Blaabjerg, R. Sebastian, J. Dannehl, and F.W. Fuchs, "Systematic design of the lead-lag network method for active damping in LCL-filter based three phase converters," *IEEE Trans. Ind. Informat.*, vol. 10, no. 1, pp. 43–52, Feb. 2014.

[10] J. Dannehl, M. Liserre, and F. W. Fuchs, "Filter-based active damping of voltage source converters with LCL filter," *IEEE Trans. Ind. Electron.*, vol. 58, no. 8, pp. 3623–3633, Aug. 2011.

[11] J. Xu, S. Xie, and T. Tang, "Active damping-based control for grid connected LCL-filtered inverter with injected grid current feedback only," *IEEE Trans. Ind. Electron.*, vol. 61, no. 9, pp. 4746–4758, Sep. 2014.

[12] X. Wang, F. Blaabjerg, and P. C. Loh, "Grid-current-feedback active damping for LCL resonance in grid-connected voltage source converters," *IEEE Trans. Power. Electron.*, vol. 31, no. 1, pp. 213–223, Jan. 2016.

[13] P. Sung-Yeul, C. Chen, L. Jih-Sheng, and M. Seung-Ryul, "Admittance compensation in current loop control for a grid-tie LCL fuel cell inverter," *IEEE Trans. Power Electron.*, vol. 23, no. 4, pp. 1716–1723, Jul. 2008.

[14] X.Wang, X. Ruan, S. Liu, and C. K. Tse, "Full feedforward of grid voltage for grid-connected inverter with LCL filter to suppress current distortion due to grid voltage harmonics," *IEEE Trans. Power Electron.*, vol. 25, no. 12, pp. 3119–3127, Dec. 2010.

[15] Y. Jia, J. Zhao, and X. Fu, "Direct grid current control of LCL-filtered grid-connected inverter mitigating grid voltage disturbance," *IEEE Trans. Power Electron.*, vol. 29, no. 3, pp. 1532–1541, Mar. 2014.

[16] S. Mukherjee, V. Roy Chowdhury, P. Shamsi and M. Ferdowsi, "Grid voltage estimation and current control of single-phase grid-connected converter without grid voltage sensor," *IEEE Trans. Power Electron.*, vol. 33, no. 5, pp. 4407 - 4418, May. 2018.

[17] S. Mukherjee, V. Roy Chowdhury, P. Shamsi, and M. Ferdowsi, "A voltage sensorless phase locked loop structure for single-phase grid connected converter system", in *proc. IEEE Energy Conversion Congress and Exposition (ECCE)*, Oct. 2017, Cincinnati, OH, USA, pp. 5720-5725.

[18] P. Rodríguez, R. Teodorescu, I. Candela, A. V. Timbus, M. Liserre, and F. Blaabjerg, "New positive-sequence voltage detector for grid synchronization of power converters under faulty grid conditions," in *Proc. 37th Annu. IEEE Power Electron. Spec. Conf.*, Jeju, Korea, Jun. 18–22, 2006, pp. 1–7.

[19] P. Rodríguez, A. Luna, M. Ciobotaru, R. Teodorescu, and F. Blaabjerg, "Advanced grid synchronization system for power converters under unbalanced and distorted operating conditions," in *Proc. 32nd IEEE IECON*, Paris, France, Nov. 6–10, 2006, pp. 5173–5178.

[20] J. A. Suul, A. Luna, P. Rodriguez, and T. Undeland, "Voltage sensor-less synchronization to unbalanced grids by frequency-adaptive virtual flux estimation," *IEEE Trans. Ind. Electron.*, vol. 59, no. 7, pp. 2910–2923, Jul. 2012.

[21] M. Malinowski, M. P. Kazmierkowski, S. Hansen, F. Blaabjerg, and G. D. Marques, "Virtual-flux-based direct power control of three-phase PWM rectifiers," *IEEE Trans. Ind. Appl.*, vol. 37, no. 4, pp. 1019–1027, Jul./Aug. 2001.

[22] L. A. Serpa, S. Ponnaluri, P. M. Barbosa, and J. W. Kolar, "A modified direct power control strategy allowing the connection of three-phase inverters to the grid through LCL-filters," *IEEE Trans. Ind. Appl.*, vol. 43, no. 5, pp. 1388–1400, Sep./Oct. 2007.